Dalton Transactions

ROYAL SOCIETY OF CHEMISTRY

PAPER

View Article Online
View Journal | View Issue

Cite this: *Dalton Trans.*, 2025, **54**, 11935

Nickel–ruthenium heterobimetallic complexes of a dinucleating unsymmetrical pincer ligand†

Vuyelwa Ngwenya, Michael A. Stevens, Michael G. Gardiner and Annie L. Colebatch *

Received 4th July 2025,
Accepted 15th July 2025

DOI: 10.1039/d5dt01568e

rsc.li/dalton

We report the first examples of complexes of an unsymmetrical, dinucelating PNNNN ligand containing a PNN pincer pocket and bidentate NN binding pocket. The proton-responsive nature of the pyrazole ligand core allows stepwise synthesis of heterobimetallic complexes *via* monometallic nickel and ruthenium complexes. Selectivity for the PNN pincer pocket is observed with Ni, whereas complexation to the bidentate NN-pocket is favoured with more sterically encumbered Ru complexes. Heterobimetallic NiFe and NiRu complexes were prepared, with metal–metal distances ranging from 3.7514(8) to 4.5305(9) Å.

Introduction

The design of bimetallic transition metal complexes is receiving considerable attention in the current literature. This stems largely from the interest in leveraging metal–metal cooperativity in catalytic processes,[1–4] inspired by the synergistic effects in multimetallic metalloenzymes that contribute to their exceptional efficiency and selectivity.[5] Heterobimetallic systems provide an additional level of tunability over homobimetallic complexes through the choice of the metal–metal pairing, but this comes with added synthetic complexities compared to homobimetallic complexes.

Heterobimetallic systems are of interest in small molecule activation[6] and catalysis,[3,4] and the use of two distinct metal sites makes heterobimetallic complexes an excellent candidate for tandem catalysis.[7] Synthetically, there are a variety of ways in which heterobimetallic complexes can be made, such as unsupported metal–metal bonded systems,[8] use of metalloligands,[9,10] or use of dinucleating ligands.[11,12] Dinucleating ligands offer advantages in terms of complex stability, metal site accessibility, and tunability of features such as the metal–metal pairing and the metal–metal distance. In particular, unsymmetrical ligands are often used to provide selectivity in the synthetic process and to afford stability to the resultant complexes, where matching of the ligand binding sites and metal fragments occurs based on features like hard–soft acid–base principles, denticity or sterics.[13–17]

N-Heteroarenes are widely used as bridging core to assemble dinucleating ligands, for example, pyrazoles, triazoles, pyridazines and naphthyridines, which give rise to metal–metal distances of around 2.5–4.5 Å.[18] Pyrazoles are attractive constructs for supporting heterobimetallic complexes as the availability of the second metal-binding site can be controlled based on the protonation state of the pyrazole, which allows for sequential metallation steps. Most dinucleating pyrazole ligands are symmetrical, such as bis(pyridyl)pyrazolate (bpp), and are used for the synthesis of homobimetallic complexes.[19] However, Hong has demonstrated the suitability of the bpp ligand system for heterobimetallic catalysts for olefin hydrogenation,[20] olefin oxidation (Fig. 1a),[21] and hydrogen peroxide production.[22]

Unsymmetrical dinucleating pyrazole ligands have been reported, including amine-phosphine,[24–27] amine-thioether,[28] and amine-cyclopentadienyl[29–31] combinations. Most relevant to this work, Akita and co-workers have reported the tetraden-

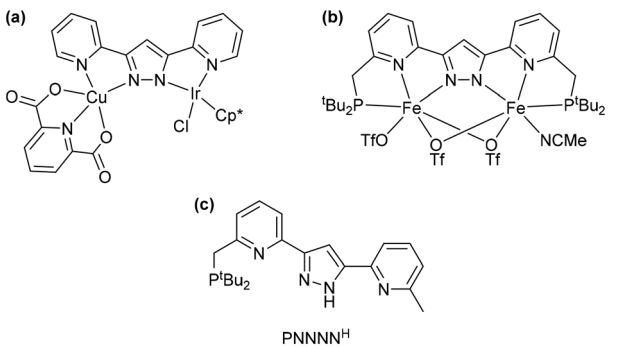

Fig. 1 (a) Example of a bpp heterobimetallic complex, reported by Hong.[21] (b) Diiron complex of the PNNNNP ligand reported by Meyer.[23] (c) The unsymmetrical PNNNN^{H} ligand studied in this work.

Research School of Chemistry, Australian National University, Canberra, ACT, 2601, Australia. E-mail: annie.colebatch@anu.edu.au

†Electronic supplementary information (ESI) available: Experimental spectra and crystallographic data. CCDC 2444593–2444599. For ESI and crystallographic data in CIF or other electronic format see DOI: https://doi.org/10.1039/d5dt01568e

tate 3-diphenylphosphinomethyl-5-pyridylpyrazole PNNN ligand, which has allowed synthesis of IrPd and IrRh heterobimetallic complexes.[24–26] Notably, through control of order of addition of reagents they were able to selectively coordinate iridium in either the PN or NN binding site.[24]

We have an ongoing interest in dinucleating ligand design.[15,32–35] Inspired by the propensity of unsymmetrical ligands to support heterobimetallic complexes,[14,15] herein we report on the coordination chemistry of an unsymmetrical PNNNN^{H} ligand (Fig. 1c). The ligand design features a pyrazole core, which allows stepwise complexation of two distinct metals, and contains a bidentate NN site and a tridentate PNN pincer site, which takes advantage of the enhanced stability and adaptability of pincer ligands.[36] PNNNN^{H} was reported by Meyer and co-workers *en route* to the symmetrical dinucleating pincer ligand PNNNNP^{H} (Fig. 1b),[23] which has featured in catalysts for N_2 silylation[37] and is capable of metal–ligand cooperativity by dearomatisation.[38] Despite the suitability of the PNNNN^{H} ligand to support heterobimetallic complexes, its coordination chemistry has not yet been explored. In this work, we report the synthesis of monometallic and heterobimetallic complexes of the PNNNN^{H} ligand bearing Ni, Fe and Ru centres.

Results and discussion

Synthesis of monometallic complexes

The PNNNN^{H} ligand was synthesised following the literature procedure reported by Meyer and co-workers.[23] Treatment of the PNNNN^{H} ligand with an equimolar amount of $NiCl_2{\cdot}6H_2O$ in MeOH yielded a mononickel complex **1** in which complexation to the PNN pincer binding pocket is observed (Scheme 1). The complex was isolated as orange crystals in 77% yield. Complex **1** is soluble in chlorinated solvents, MeCN, MeOH, DMF and DMSO and is stable under ambient conditions. The ^{1}H NMR spectrum of **1** shows 7 proton environments in the aromatic region that agree with the ligand protons and a singlet observed at 2.65 ppm that corresponds to the methyl protons. The methylene and *tert*-butyl protons were also observed as singlets at 3.65 ppm and 1.65 ppm, respectively, with no visible $^{3}J_{PH}$ coupling, as seen in related [NiCl(PNN)]Cl pincer complexes.[39] The ^{31}P NMR spectrum showed a broad signal at 78.8 ppm, shifted 40 ppm downfield from that observed for the free ligand, again consistent with related Ni-pincer compounds.[39] High resolution mass spectrometry and X-ray crystallography also confirmed the formation of complex **1**.

Yellow crystals of **1** were grown by layering a chloroform solution of complex **1** with *n*-hexane. The molecular structure (Fig. 2) illustrates the PNN chelation coordination mode of the ligand and the square planar geometry at Ni (τ_4 0.11)[40] is consistent with the observed diamagnetism of the complex. The Ni–N4(pyridine), Ni–N3(pyrazole), Ni–Cl1 and Ni–P1 distances were found to be 1.890(2) Å, 1.945(2) Å, 2.1395(9) Å and 2.1695 (8) Å respectively, which resemble those observed in other Ni-PNN pincer complexes.[39]

While selectivity for the PNN pincer pocket was observed for Ni, selectivity can be switched to favour the NN pocket by use of a more sterically encumbered complex. This was demonstrated by reaction of PNNNN^{H} with $RuCl_2(PPh_3)_3$, from which the NN-bound complex **2** could be isolated in 84% crystalline yield (Scheme 1). The ^{1}H NMR spectrum of **2** shows no difference in the chemical shift of the *tert*-butyl and CH_2 resonances of the ligand upon Ru complexation. However, the CH_3 peak has shifted upfield from 2.60 ppm to 1.27 ppm, thereby confirming the coordination of Ru in the NN pocket. Similarly, the ^{31}P NMR resonance of the ligand is largely unchanged (36.3 ppm in **2** *cf.* 36.8 ppm in PNNNN^{H}). An additional signal is observed at 23.2 ppm corresponding to the two-equivalent *trans* PPh_3 groups. The solid-state structure of **2** is shown in Fig. 3. The structure confirms the N,N-coordination mode, with an observed bite angle of N1–Ru1–N2 77.2(1)°. The Ru1–N1(pyridyl) bond length (2.186(3) Å) is noticeably longer than the Ru1–N2(pyrazole) bond length (1.999(3) Å), consistent with the stronger bonding of pyrazole.[41–43]

While $RuCl_2(PPh_3)_3$ has been used previously in the synthesis of 2,6-bis(pyrazole)pyridine pincer complexes,[44,45] in this case no coordination to the PNN pincer pocket of the PNNNN^{H} ligand was observed. When the precursor RuHCl(CO)$(PPh_3)_3$ was used, which has been used extensively to synthesise pincer complexes,[46–49] an NN-bound complex [RuH

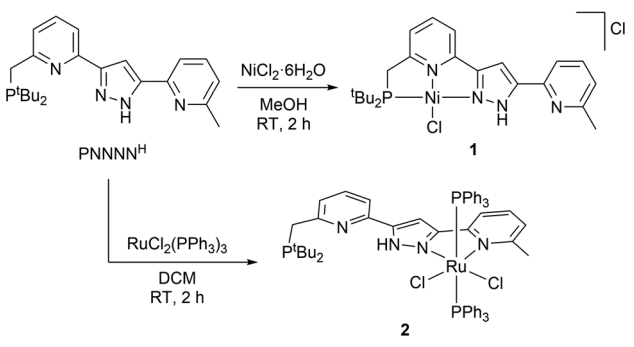

Scheme 1 Synthesis of monometallic complexes **1** and **2**.

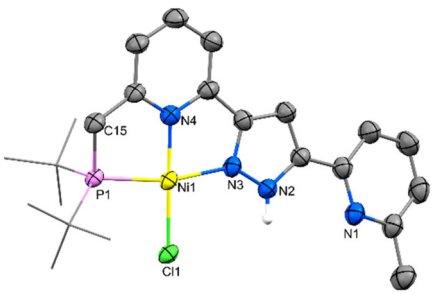

Fig. 2 X-ray crystal structure of **1** (50% displacement ellipsoids, selected hydrogen atoms and Cl^- anion omitted). Selected bond lengths (Å) and angles (°): Ni1–P1 2.1695(8), Ni1–N3 1.945(2), Ni1–N4 1.890(2), Ni1–Cl1 2.1395(9), N4–Ni1–Cl1 178.20(7), P1–Ni1–N3 165.90(7).

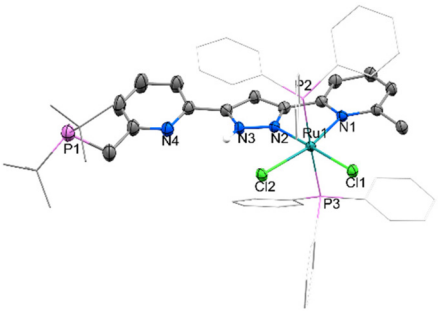

Fig. 3 X-ray crystal structure of **2** (50% displacement ellipsoids, selected hydrogen atoms and DCM solvent omitted). Selected bond lengths (Å) and angles (°): Ru1–N1 2.186(3), Ru1–N2 1.999(3), Ru1–Cl1 2.443(1), Ru1–Cl2 2.452(1), Ru1–P2 2.3629(9), Ru1–P3 2.3842(9), N1–Ru1–N2 77.2(1).

$(CO)(PPh_3)_2(N,N'\text{-PNNNN}^H)]Cl$ (**3**) was again observed as the major product (Scheme S1†). This was identified based on similar ^{31}P NMR resonance of 36.3 ppm (P^tBu_2) to **2**, as well as the ^1H NMR shift of the CH_3 moiety (1.76 ppm). However, the NMR spectra contained additional resonances and unfortunately, we were unable to isolate a pure compound. Crystals suitable for X-ray crystallographic analysis were obtained, the structure of which was identified as $[RuH(CO)(PPh_3)_2(N,N'\text{-PNNNN}^H)]Cl$ (Fig. S30†). Unfortunately, despite repeated attempts we were unable to obtain these on a bulk scale.

Synthesis of heterobimetallic complexes

One of the advantages of the pyrazole ligand core is the ability to control whether the ligand acts as a mononucleating or dinucleating ligand based on its protonation state. Proton-responsive ligands have been used to afford structural control over nuclearity,[35,50,51] in so-called structurally-responsive behaviour.[52] Deprotonation of the monometallic complexes will make the second metal binding site available, which is currently masked by protonation in complexes **1** and **2**, thereby allowing formation of heterobimetallic complexes. Despite the prevalence of pyrazolate ligands, there are only two reports in the literature of pyrazolate being used to bridge NiRu complexes,[53,54] and two examples of pyrazolate-bridged NiFe systems, both of which form tetranuclear assemblies.[55,56]

Complex **1** was treated with one equivalent of $FeCl_2{\cdot}4H_2O$ in methanol at room temperature in the presence of NEt_3 to yield a paramagnetic mixture that was poorly soluble and difficult to purify or characterise. From this, the heterobimetallic NiFe complex **4** (Scheme 2) was able to be identified crystallographically from crystals grown from MeCN/Et_2O. The molecular structure (Fig. 4a) shows the Fe bound in the NN pocket in a pseudo-tetrahedral geometry (τ_4 = 0.87).[40] The distance between the Ni and Fe centres was found to be 4.125(1) Å, slightly longer than that in the FeNi(μ-CN)(bpp) fragment of the reported Fe_2Ni_2 grid (4.0438(8) Å).[55] Similar to **2**, the Fe1–N1(pyridyl) distance is significantly longer than the Fe1–N2 (pyrazolate) distance (2.240(4) *cf.* 2.059(3) Å, respectively), and the N1–Fe1–N2 bite angle was found to be 76.0(1)°. It is notable that the PNNNN ligand restricts the nuclearity of the complex to a bimetallic system, rather than the tetrametallic examples that have been seen in the literature previously for NiFe complexes of bpp and other dinucleating pyrazolate derivatives.[55,56]

Because of the difficulties in obtaining a NiFe complex on a bulk scale, our focus shifted to more soluble, diamagnetic Ru systems. A NiRu complex **5** was prepared by stirring the mononickel precursor **1** with one equivalent of $RuHCl(CO)(PPh_3)_3$ and excess NEt_3 in THF at 65 °C (Scheme 2). The ^1H NMR spectrum of **5** shows a characteristic Ru–H triplet resonance at −10.06 ppm ($^2J_{PH}$ = 18.7 Hz) due to the presence of the two magnetically equivalent *trans* PPh_3 ligands.[57] Interestingly, while $^3J_{PH}$ coupling in the $PNNNN^H$ ligand was not observed in the precursor **1**, upon complexation of Ru to the distal NN site these couplings are resolved, with coupling observed for both the CH_2 ($^3J_{PH}$ = 10.8 Hz) and ^{t}Bu ($^3J_{PH}$ = 14.6 Hz) signals. The ^{31}P NMR spectrum contains two singlets: one at 43.3 ppm corresponding to the *trans* PPh_3 ligands and another one at 62.2 ppm corresponding to the PNNNN phosphine arm. The

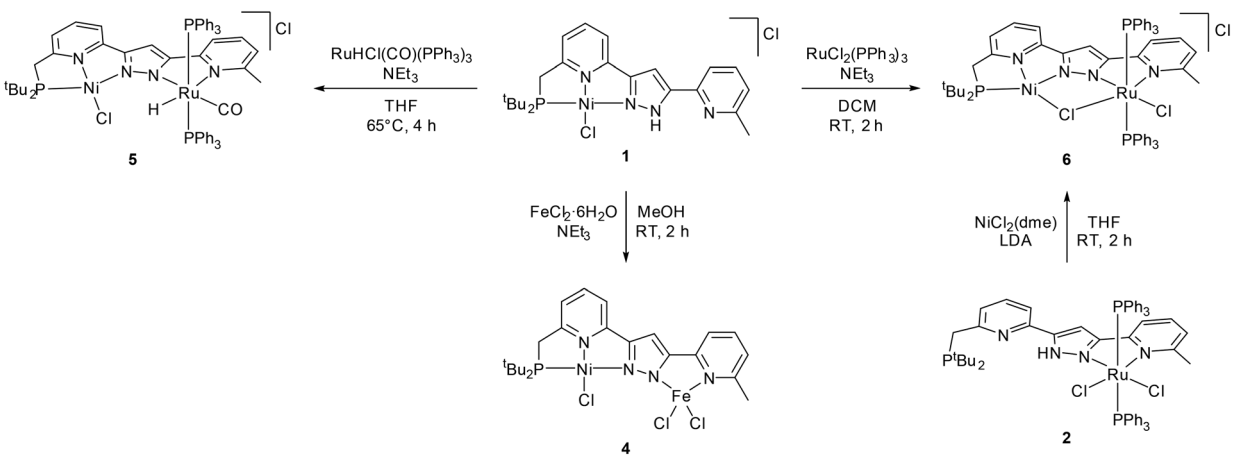

Scheme 2 Synthesis of heterobimetallic complexes **4**, **5** and **6**.

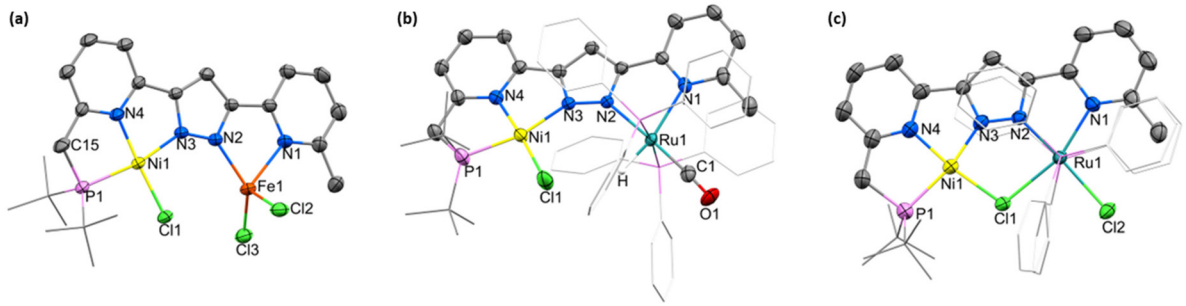

Fig. 4 X-ray crystal structures of (a) **4**, (b) **5**, and (c) **6**. 50% displacement ellipsoids, selected hydrogen atoms, solvent and non-coordinating anions omitted. Selected bond lengths (Å) and angles (°): **4**: Ni1···Fe1 4.125(1), Ni1–P1 2.174(1), Ni1–N3 1.892(2), Ni1–N4 1.889(4), Fe1–N1 2.240(4), Fe1–N2 2.059(3). **5**: Ni1···Ru1: 4.5305(9), Ni1–Cl1 2.126(1), Ni1–P1 2.178(1), Ni1–N3, 1.993(3), Ni1–N4 1.893(2), Ru1–N1 2.257(3), Ru1–N2 2.146(2), N3–Ni1–N4 83.6(1), N1–Ru1–N2 76.8(1). **6**: Ni1···Ru1: 3.7514(8), Ni1–Cl1 2.198(1), P1–Ni1 2.189(1), Ni1–N3 1.843(3), Ni1–N4 1.891(3), Ru1–Cl1 2.5168(8), Ru1–Cl2 2.457(1), Ru1–N1 2.150(3), Ru1–N2 1.953(3), Ni1–Cl1–Ru1 105.25(4), N3–Ni1–N4 81.4(1), N1–Ru1–N2 76.9(1).

FTIR spectrum of the complex showed a strong absorption band at around 2078 cm^{-1} which was assigned to the CO stretch therefore asserting the presence of the CO ligand.

Crystals suitable for X-ray analysis were grown from layering a chloroform solution of complex **5** with *n*-hexane. The molecular structure of **5** (Fig. 4b) shows Ru coordinated in the NN pocket in an octahedral geometry. The hydride and the CO ligands lie in the equatorial plane with the expected *cis*-H-Ru-pyrazolate arrangement. No H/CO positional disorder was evident, consistent with the observation of a single isomer spectroscopically. The distance between Ni and Ru was found to be 4.5305(9) Å, which was larger than the nickel–iron distance in **4** of 4.125(1) Å, possibly due to the increased steric bulk around Ru in **5** compared to that around Fe in **4**, and repulsion between the chloride and hydride ligands that both point towards the pocket. The metal–metal distances in **3** and **4** are comparable to those in Akita's IrPd(PNNN)(COD)(allyl) heterobimetallic systems of 4.292(4)–4.639(3) Å.[24] The distances between Ru1–N1(pyridyl) and Ru1–N2(pyrazolate) were found to be 2.257(3) Å and 2.146(2) Å, respectively, in line with the stronger bonding of the anionic pyrazolate ligand than the neutral pyridyl ligand.

When $RuCl_2(PPh_3)_3$ was used in place of $RuHCl(CO)(PPh_3)_3$, a heterobimetallic NiRu complex was obtained containing a bridging μ-Cl ligand (complex **6**, Scheme 2). Complex **6** could be synthesised in two ways, as shown in Scheme 2. The first method involved treating **1** with one equivalent of $RuCl_2(PPh_3)_3$ in DCM in the presence of excess NEt_3 at room temperature for two hours. In the alternative method, the monoruthenium complex **2** was reacted with one equivalent of $NiCl_2$(dme) in the presence of LDA in THF to form complex **6**. Complex **6** was obtained as green, air-sensitive crystals. The ^{31}P NMR spectrum of **6** shows no significant difference in the PPh_3 chemical shift compared to that of **2**. However, a downfield shift of the PNNNN phosphine resonance from 36.3 ppm in **2** to 71.1 ppm in **6** is observed, close to that of the mononickel precursor **1** (76.9 ppm), therefore confirming the PNN ligation of Ni.

The solid-state structure of **6** shows Ni in a square planar geometry (τ_4 = 0.14)[40] in the PNN pocket and Ru in the NN pocket in an octahedral geometry, with a chloride ligand bridging the two metals (Fig. 4c). The Ni···Ru distance was found to be 3.7514(8) Å, which was the shortest distance of the three heterobimetallic complexes. Notably, this is the shortest metal–metal distance for bpp-type ligands, with the previous shortest reported distance being 3.785(1) Å in the peroxo-bridged dicobalt(III) complex $[Co_2(\mu\text{-bpp})(\mu\text{-}1,2\text{-}O_2)(Me_2bimpy)_2][PF_6]_3$.[58] As expected, the distance is well beyond the sum of the covalent radii of Ni and Ru ($\sum r_{cov} = 2.70$ Å), indicative of the absence of any metal–metal interaction. The Ru1–Cl1 (2.5168(8) Å) distance is slightly longer than sum of the covalent radii (2.48 Å), whereas the Ni1–Cl1 distance (2.198(1) Å) is within the sum of the covalent radii (2.26 Å), suggesting a stronger Ni–Cl interaction.[59] A contraction of the Ni1–N3 distance is observed upon Ru complexation, from 1.945(2) Å in **1** to 1.843(3) Å in **6**. This is ascribed to constraints imparted by the Ni(μ-Cl)Ru arrangement, as the Ni1–N3 distance lengthens upon Ru complexation in **5** to 1.993(3) Å.

Electrochemical studies

Cyclic voltammetry (CV) of complexes **1**, **2**, **5** and **6** was investigated. CV studies were conducted in dry MeCN containing 0.1 M $N^nBu_4PF_6$ at 0.1 mV s^{-1}, with all potentials measured with reference to Fc/Fc^+. Measurements at increasing scan rates showed that the peak currents for the reduction/oxidation waves follow the Randles–Ševčík equation, indicating that mass transport is diffusion controlled in solution. Anodic scans of **1**, **5** and **6** are obscured by oxidation of the chloride counterion at $E_{pa} \approx 0.65$ V.

Complex **1** shows two successive quasi-reversible reductions at $E_{1/2}$ = −1.22 V and −1.39 V (Fig. S9†). One of these is presumed to correspond to the $Ni^{II/I}$ event, but is not possible to assign without further information, especially given the proximity of the events. $Ni^{II/I}$ reductions are observed across a wide range in pincer complexes, including −1.90 V (THF, *vs.* Fc/Fc^+) for the cyclometallated complex NiBr(Phbpy) (Phbpy = 2,2′-bipyridine-6-phen-2-yl),[60] −2.28 V (THF, *vs.* Fc/Fc^+) in NiCl(^{acr}PNP) (^{acr}PNP = 4,5-bis(di-iso-propylphosphino)-2,7,9,9-

tetramethyl-9*H*-acridin-10-ide)[61] or −1.20 V (THF, *vs.* Fc/Fc^+) or −1.34 V (MeCN, *vs.* Fc/Fc^+) for the cationic complexes [Ni(CO)(^{acr}PNP)]BF_4[62] and [NiCl(PNP)]BAr^F_4 (PNP = 2,6-bis{(di-*tert*-butylphosphino)propyl}pyridine),[63] respectively. The nature of the second reduction remains inconclusive at this stage.

The electrochemical profile of complex **2** shows no peaks in the cathodic region. However, upon scanning in the anodic direction two minor irreversible oxidation peaks are observed at E_{pa} = 0.42 V and 0.51 V (Fig. S19†). Another reversible redox process was observed at $E_{1/2}$ = 0.72 V (ΔE = 76 mV) which was assigned the $Ru^{III/II}$ couple. This is supported by comparisons to reported $Ru^{III/II}$ data in the literature, such as 0.78 V (MeCN, *vs.* Fc/Fc^+) in $[Ru(N_4)(pic)_2][PF_6]_2$ (N_4 = 6,6′-di(1*H*-pyrazol-3-yl)-2,2′-bipyridine, pic = 4-picoline)[64] or 0.52 V (DCM, *vs.* Fc/Fc^+) for the pyridyl-bis(pyrazole) complex $[RuCl(NNN)(PPh_3)_2]Cl$.[65]

Notably, scanning the CV of complex **6** to −2 V shows no cathodic processes (Fig. S40†), indicating that $Ni^{II/I}$ reduction in this bimetallic complex is significantly more difficult. This may arise from the coordination of the anionic form of the PNNN ligand and change in geometry to accommodate the bridging chloride ligand. The bimetallic complex **5**, in which the Ni–Cl ligand remains terminal, shows an irreversible reduction at −1.59 V (Fig. S30†), which might suggest the bridging *vs.* terminal nature of the chloride ligand impacts the redox chemistry at Ni.

Conclusions

In this work, we have demonstrated the suitability of unsymmetrical pyrazolate ligands for the controlled synthesis of heterobimetallic complexes. The proton-responsive nature of the $PNNNN^H$ ligand has been successfully utilised to control nuclearity, while site-selectivity for formation of PNN- *vs.* NN-bound monometallic complexes is achieved through the choice of the metal precursor, in this case *via* steric control. The PNNNN ligand supports a range of metal–metal distances, from 4.5305(9) Å in **5** to 3.7514(8) Å in **6**, the shortest reported metal–metal distance for bis(pyridyl)pyrazolyl-type ligands to date. Applying these approaches in future will provide access to a wide range of metal–metal combinations and co-ligand arrangements in homo- and heterobimetallic complexes towards the application of bimetallics in reactivity, catalysis and for their electrochemical, photophysical and magnetic properties.

Experimental

General considerations

Unless stated otherwise, all reactions were carried out using standard Schlenk and glovebox techniques under a dry, oxygen-free atmosphere. All solvents were dried and degassed prior to use. $PNNNN^H$,[23] $RuHCl(CO)(PPh_3)_3$,[66] and $RuCl_2(PPh_3)_3$[67] were synthesised according to literature procedures. All other reagents were obtained from commercial sources and used as received.

NMR data were collected at 25 °C on a Bruker Avance 400 (^{1}H at 400 MHz, $^{31}P\{^1H\}$ at 162 MHz, $^{13}C\{^1H\}$ at 101 MHz), Bruker Avance 600 (^{1}H at 600 MHz, $^{13}C\{^1H\}$ at 151 MHz), Bruker Avance 700 (^{1}H at 700 MHz, $^{31}P\{^1H\}$ at 284 MHz, $^{13}C\{^1H\}$ at 176 MHz) or Bruker Avance 800 (^{1}H at 800 MHz, $^{13}C\{^1H\}$ at 201 MHz). Chemical shifts (δ) are reported in ppm and coupling constants given in Hz, with referencing to the residual solvent peak for ^{1}H and ^{13}C and an external H_3PO_4 reference for ^{31}P NMR. Stated multiplicities are of the primary resonance and are represented by the abbreviations s (singlet), d (doublet), t (triplet), m (multiplet), and combinations thereof. Coupling between nuclei, $^nJ_{AB}$, are reported in Hz.

Electrospray Ionisation Mass Spectrometry (ESI-MS) was performed at the ANU Joint Mass Spectrometry Facility, using acetonitrile or methanol as the matrix. UV/Vis spectra were recorded on a PerkinElmer Lambda 465 spectrometer. Infrared spectra were recorded on a PerkinElmer FTIR spectrometer.

X-ray crystallographic data were collected on an Agilent SuperNova diffractometer using Cu-Kα (λ = 1.54184 Å) radiation and data reduction, and finalisation was done using the CrysAlis PRO software.[68] The structures were solved by direct or Patterson methods and refined by full-matrix least-squares on F^2 using the SHELXT and SHELXL programs with the Olex2 interface.[69–71] Hydrogen atoms were placed at calculated positions and refined using a riding model.

Cyclic voltammetry experiments were performed using a Metrohm Autolab PGSTAT204 potentiostat and carried out in dry MeCN under N_2 in a single-compartment three-electrode glass cell with a glassy carbon working electrode (3 mm diameter), a Pt wire counter electrode, and a silver wire in a ceramic-fritted glass tube filled with electrolyte as a pseudo-reference electrode. Electrodes and cells were purchased from Gaoss Union. Pseudo-reference potentials were referenced to Fc added into the analyte solution following completion of each measurement. The supporting electrolyte was 0.1 M $N^nBu_4PF_6$, and the analyte concentration was 1.0 mM.

Synthesis of [NiCl($PNNNN^H$)]Cl (1)

$PNNNN^H$ (100.0 mg, 0.2535 mmol) and $NiCl_2{\cdot}6H_2O$ (60.3 mg, 0.254 mmol) were stirred in dry methanol for 2 h under nitrogen. After 2 h, the methanol was removed *in vacuo*. Bulk orange crystals suitable for X-ray crystallographic analysis were obtained by layering a $CHCl_3$ solution of the complex with *n*-hexane at room temperature. Crystalline yield: 102.3 mg, 0.1952 mmol, 77%. ^{1}H NMR (400 MHz, CD_3OD, ppm): δ = 8.15 (dd, $^3J_{HH}$ = 7.8 Hz, H12, 1H), 7.9 (dd, $^3J_{HH}$ = 7.9 Hz, H4, 1H), 7.88 (d, $^3J_{HH}$ = 7.7 Hz, H13, 1H) 7.83 (d, $^3J_{HH}$ = 7.8 Hz, H11, 1H), 7.59 (d, $^3J_{HH}$ = 7.9 Hz, H5, 1H), 7.57 (s, H8, 1H), 7.41 (d, $^3J_{HH}$ = 7.7 Hz, H3, 1H), 3.84 (s, CH_2, 2H), 2.65 (s, CH_3, 3H), 1.65 (s, ^{t}Bu, 18H). ^{31}P NMR (162 MHz, CD_3OD, ppm): δ = 78.8 (s, broad). ^{13}C NMR (201 MHz, CD_3OD, ppm): δ = 164.2 (d, $^2J_{CP}$ = 6.7 Hz, C14), 158.4 (s, C2), 151.6 (s, C9), 150.4 (s, C10), 146.6 (s, C7), 145.3 (s, C6), 141.6 (s, C12), 139.0 (s, C4), 124.5 (s, C3), 123.2 (s, C13), 119.4 (s, C11), 119.1 (s, C5), 102.5 (s, C8), 36.2 (b, ^{t}Bu–C), 33.8 (s, CH_2), 27.7 (s, ^{t}Bu–CH_3), 22.2 (s, CH_3). MS-ESI(+) (*m*/*z*): calculated for $[C_{23}H_{31}N_4ClNiP]^+$ 487.1323. Found 487.1383. UV/Vis (CH_3CN, λ_{max} (nm), ε (M^{-1} cm^{-1})): 253 (30 700), 276 (33 500), 315 (38 200).

Synthesis of $[RuCl_2(PPh_3)_2(PNNNN^H)]$ (2)

$PNNNN^H$ (50.0 mg, 0.1267 mmol) and $RuCl_2(PPh_3)_3$ (121.5 mg, 0.2535 mmol) were stirred in DCM for 2 h under nitrogen. After 2 h, the solution was concentrated *in vacuo* and *n*-hexane was added to precipitate the product. The bright yellow precipitate was isolated by filtration and washed twice with *n*-hexane to remove free PPh_3. The yellow compound was then recrystalised by layering a concentrated DCM solution of the complex with *n*-hexane. Crystalline yield 116.3 mg, 0.1066 mmol, 84%. ^{1}H NMR (400 MHz, CD_2Cl_2, ppm): δ = 11.72 (s, NH, 1H), 7.59 (dd, J = 7.8 Hz, Ar, 1H), 7.50 (dd, J = 7.6 Hz, Ar, 1H), 7.37–7.47 (m, Ar, 15H), 7.34 (d, J = 7.5 Hz, Ar, 1H), 6.98–7.14 (m, Ar, 15H), 6.55 (d, J = 7.7 Hz, Ar, 1H), 6.48 (s, CH, 1H), 3.07 (d, $^2J_{PH}$ = 3.2 Hz, 2H, CH_2), 1.35 (s, 3H, CH_3), 1.19 (d, $^3J_{PH}$ = 11.0 Hz, 18H, ^{t}Bu). ^{31}P NMR (162 MHz, CD_2Cl_2, ppm): δ = 36.3 (s, P(^{t}Bu)$_2$), 23.2 (s, PPh_3). ^{13}C NMR (201 MHz, CD_2Cl_2, ppm): 172.3 (s, Ar), 163.1 (s, Ar), 154.4 (s, Ar), 153.1 (s, Ar), 145.4 (s, Ar), 143.2 (s, Ar), 137.7 (s, Ar), 137.0 (s, Ar), 134.7 (vt, J = 5.1 Hz, Ar), 134.6 (vt, J = 26.4 Hz, Ar), 128.9 (s, Ar), 127.6 (vt, J = 4.1 Hz, Ar), 123.7 (s, Ar), 116.4 (s, Ar), 115.5 (s, Ar), 100.3 (s, CH_{pz}), 36.5 (^{t}Bu–C), 31.9 (m, CH_2), 29.5 (d, J_{CP} = 13.4 Hz, ^{t}Bu–CH_3), 26.9 (s, CH_3). MS-ESI(+) (m/z): calculated for $[C_{61}H_{64}N_5ClRuP_3]^+$ 1096.3102. Found 1096.3116 $[M + CH_3CN]^+$. UV/Vis (CH_3CN, λ_{max} (nm), ε (M^{-1} cm^{-1})): 271 (35 200), 323 (38 800).

Synthesis of $[NiClRuH(CO)(PPh_3)_2(PNNNN)]Cl$ (5)

Complex **1** (100.0 mg, 0.2535 mmol), $RuHCl(CO)(PPh_3)_3$ (120.5 mg, 0.5070 mmol) and LDA (2.0 M in THF/heptane/ethylbenzene, one drop) were stirred in THF for 4 h at 65 °C under nitrogen. After 4 h, the reaction mixture was filtered to remove the salts. The reaction mixture was then concentrated, and *n*-hexane was added to precipitate a salmon residue. The product was then isolated by filtration and washed twice with *n*-hexane to remove free PPh_3. Red crystals suitable for X-ray crystallographic analysis were obtained by layering a $CHCl_3$ solution of the complex with *n*-hexane at room temperature. Crystalline yield: 58.2 mg, 0.494 mmol, 52%. ^{1}H NMR (400 MHz, $CDCl_3$, ppm): δ = 7.94 (dd, J = 7.2 Hz, Ar, 1H), 7.75 (d, J = 7.8 Hz, Ar, 1H), 7.55 (m, Ar, 2H), 7.35–7.41 (m, Ar, 13H), 7.16–7.21 (m, Ar, 18H), 6.92 (s, pz-CH, 1H), 6.75 (d, J = 7.8 Hz, Ar, 1H), 3.53 (d, $^2J_{PH}$ = 10.8 Hz, CH_2, 2H), 1.56 (s, CH_3, 3H), 1.43 (d, $^3J_{PH}$ = 14.6 Hz, ^{t}Bu, 18H), −10.13 (t, $^2J_{PH}$ = 18.7 Hz, Ru–H, 1H). ^{31}P NMR (162 MHz, $CDCl_3$, ppm): δ = 62.2 (s, P(^{t}Bu)$_2$), 43.3 (s, PPh_3). ^{13}C NMR (201 MHz, $CDCl_3$, ppm): δ = 162.4 (s, Ar), 160.9 (s, Ar), 154.0 (s, Ar), 153.2 (s, Ar), 151.3 (s, J = 16.9 Hz, Ar), 141.5 (s, Ar), 136.7 (s, Ar), 134.2 (vt, J = 21.0 Hz, Ar), 133.9 (vt, J = 5.8 Hz, Ar), 129.4 (s, Ar), 128.0 (vt, J = 4.6 Hz, Ar), 123.7 (s, Ar), 121.5 (d, J = 8.4 Hz, Ar), 117.4 (s, Ar), 117.0 (s, Ar), 103.2 (s, pz-CH), 36.7 (d, $^1J_{CP}$ = 18.2 Hz, ^{t}Bu–C), 34.6 (d, $^1J_{CP}$ = 21.9 Hz, CH_2), 29.2 (s, ^{t}Bu–CH_3), 27.1 (s, CH_3). Ru–CO not observed. MS-ESI(+) (m/z): calculated for $[C_{60}H_{61}ClN_4NiOP_3Ru]^+$ 1141.2139. Found 1141.2142. UV/Vis (CH_3CN, λ_{max} (nm), ε (M^{-1} cm^{-1})): 253 (26 900), 272 (28 900), 323 (34 300).

Synthesis of $[NiRuCl_2(PPh_3)_2(PNNNN)]Cl$ (6)

Method (A): Complex **1** (90.0 mg, 0.172 mmol), $RuCl_2(PPh_3)_3$ (165.0 mg, 0.172 mmol) and excess NEt_3 (1 drop) were stirred in DCM for 2 h under nitrogen. After 2 h, the solution mixture was filtered before it was concentrated *in vacuo* and *n*-hexane added to precipitate the product. It was then isolated by filtration and washed twice with *n*-hexane to remove free PPh_3. THF was then added to the residue and sonicated and filtered to remove the NEt_3HCl salt. The green compound was then recrystallised by layering a concentrated DCM solution of the complex with *n*-hexane. Crystalline yield: 113.3 mg, 0.9568 mmol, 56%. **Method (B):** Complex **2** (50 mg, 0.0458 mmol) was reacted with $NiCl_2$(dme) (10.1 mg, 0.0458 mmol) in THF in the presence of LDA (2.0 M in THF/heptane/ethylbenzene, one drop) for 2 h at room temperature. After 2 h, the solution mixture was filtered, concentrated and then layered with *n*-hexane to obtain green crystals of **5** which were washed with diethyl ether before drying. Crystalline yield: 41.2 mg, 0.348 mmol, 76%. ^{1}H NMR (400 MHz, CD_2Cl_2, ppm): δ = 7.97 (s, Ar, 1H), 7.67 (s, Ar, 1H), 7.50–7.54 (m, Ar, 13H), 7.22–7.25 (m, Ar, 6H), 7.09–7.13 (m, Ar, 14H), 6.58 (d, $^3J_{HH}$ = 7.5 Hz, Ar, 1H), 6.22 (s, pz-CH, 1H), 3.80 (d, $^2J_{PH}$ = 7.6 Hz, CH_2), 1.52 (s, CH_3, 3H), 1.22 (d, $^3J_{PH}$ = 14.7 Hz, ^{t}Bu, 18H). ^{31}P NMR (162 MHz, CD_2Cl_2, ppm): δ = 71.1 (s, P(^{t}Bu)), 24.2 (s, PPh_3). ^{13}C NMR (201 MHz, CD_2Cl_2, ppm): δ = 172.0 (s, Ar), 164.9 (s, Ar), 158.7 (s, Ar), 154.0 (s, Ar), 150.3 (s, Ar), 148.8 (s, Ar), 142.6 (s, Ar), 136.1 (s, Ar), 134.7 (vt, J = 5.2 Hz, Ar), 133.4 (vt, J = 18.7 Hz, Ar), 129.6 (s, Ar), 127.9 (vt, J = 4.3 Hz, Ar), 125.0 (s, Ar), 122.6 (s, Ar), 117.6 (s, Ar), 116.7 (s, Ar), 102.0 (pz-CH), 35.7 (d, $^1J_{CP}$ = 17.2 Hz, ^{t}Bu–C) 35.0 (br, CH_2), 28.6 (s, ^{t}Bu–CH_3), 27.8 (s, CH_3). MS-ESI(+) (m/z): calculated for $[C_{59}H_{60}Cl_2N_4NiP_3Ru]^+$ 1147.1800. Found 1147.1829. UV/Vis (CH_3CN, λ_{max} (nm), ε (M^{-1} cm^{-1})): 273 (31 500), 320 (20 900).

Author contributions

Synthesis and characterisation were performed by VN. X-ray crystallographic analysis was conducted by VN, MAS and MGG. Data analysis was conducted by VN and ALC. Supervision was conducted by MAS and ALC. Project conceptualisation, oversight and funding acquisition were conducted by ALC. The manuscript was written by VN and ALC.

Conflicts of interest

There are no conflicts to declare.

Data availability

The data supporting this article have been included as part of the ESI.† Crystallographic data for $PNNNN^H$, **1**, **2**, **3**, **4**, **5** and **6** have been deposited in the CCDC 2444593–2444599.†

Acknowledgements

Technical support from Anitha Jeyasingham and Dr Doug Lawes, and financial support from the Australian Research Council (DE200100450), is gratefully acknowledged.

References

1 R. Maity, B. S. Birenheide, F. Breher and B. Sarkar, *ChemCatChem*, 2021, **13**, 2337–2370.
2 M. A. Stevens and A. L. Colebatch, *Chem. Soc. Rev.*, 2022, **51**, 1881–1898.
3 Z. Fickenscher and E. Hey-Hawkins, *Molecules*, 2023, **28**, 4233.
4 P. C. Abhyankar and C. M. Thomas, *Angew. Chem., Int. Ed.*, 2024, **63**, e202416100.
5 A. C. Ghosh, C. Duboc and M. Gennari, *Coord. Chem. Rev.*, 2021, **428**, 213606.
6 R. Govindarajan, S. Deolka and J. R. Khusnutdinova, *Chem. Sci.*, 2022, **13**, 14008–14031.
7 R. C. Nishad, S. Kumar and A. Rit, *Organometallics*, 2021, **40**, 915–926.
8 S. Banerjee, M. K. Karunananda, S. Bagherzadeh, U. Jayarathne, S. R. Parmelee, G. W. Waldhart and N. P. Mankad, *Inorg. Chem.*, 2014, **53**, 11307–11315.
9 N. Hara, T. Saito, K. Semba, N. Kuriakose, H. Zheng, S. Sakaki and Y. Nakao, *J. Am. Chem. Soc.*, 2018, **140**, 7070–7073.
10 B. L. Ramirez and C. C. Lu, *J. Am. Chem. Soc.*, 2020, **142**, 5396–5407.
11 A. C. Deacy, A. F. R. Kilpatrick, A. Regoutz and C. K. Williams, *Nat. Chem.*, 2020, **12**, 372–380.
12 S.-Y. Liu, G. H. Maunder, A. Sella, M. Stevenson and D. A. Tocher, *Inorg. Chem.*, 2002, **35**, 76–81.
13 S. Maggini, *Coord. Chem. Rev.*, 2009, **253**, 1793–1832.
14 S. Deolka, O. Rivada-Wheelaghan, S. L. Aristizábal, R. R. Fayzullin, S. Pal, K. Nozaki, E. Khaskin and J. R. Khusnutdinova, *Chem. Sci.*, 2020, **11**, 5494–5502.
15 J. Wu, M. A. Stevens, M. G. Gardiner and A. L. Colebatch, *Dalton Trans.*, 2024, **53**, 18037–18046.
16 A. Nicolay and T. D. Tilley, *Chem. – Eur. J.*, 2018, **24**, 10329–10333.
17 P. L. Dunn, R. K. Carlson, L. Gagliardi and I. A. Tonks, *Dalton Trans.*, 2016, **45**, 9892–9901.
18 A. L. Gavrilova and B. Bosnich, *Chem. Rev.*, 2004, **104**, 349–383.
19 J. Klingele, S. Dechert and F. Meyer, *Coord. Chem. Rev.*, 2009, **253**, 2698–2741.
20 D. Hong, Y. Ohgomori, Y. Shimoyama, H. Kotani, T. Ishizuka, Y. Kon and T. Kojima, *Inorg. Chem.*, 2019, **58**, 11284–11288.
21 Y. Shimoyama, Y. Kitagawa, Y. Ohgomori, Y. Kon and D. Hong, *Chem. Sci.*, 2021, **12**, 5796–5803.
22 Y. Shimoyama, Y. Ohgomori, Y. Kon and D. Hong, *Dalton Trans.*, 2021, **50**, 9410–9416.
23 S. Samanta, S. Demesko, S. Dechert and F. Meyer, *Angew. Chem., Int. Ed.*, 2015, **54**, 583–587.
24 C. Dubs, A. Inagaki and M. Akita, *Chem. Commun.*, 2004, 2760–2761.
25 C. Dubs, T. Yamamoto, A. Inagaki and M. Akita, *Organometallics*, 2006, **25**, 1344–1358.
26 C. Dubs, T. Yamamoto, A. Inagaki and M. Akita, *Organometallics*, 2006, **25**, 1359–1367.
27 M. Konrad, S. Wuthe, F. Meyer and E. Kaifer, *Eur. J. Inorg. Chem.*, 2001, **2001**, 2233–2240.
28 J. C. Röder, F. Meyer, M. Konrad, S. Sandhöfner, E. Kaifer and H. Pritzkow, *Eur. J. Org. Chem.*, 2001, 4479–4487.
29 J. C. Röder, F. Meyer, R. F. Winter and E. Kaifer, *J. Organomet. Chem.*, 2002, **641**, 113–120.
30 T. Sheng, S. Dechert, A. C. Stückl and F. Meyer, *Eur. J. Inorg. Chem.*, 2005, **2005**, 1293–1302.
31 H. Zhang, S. Dechert, M. Linseis, R. F. Winter and F. Meyer, *Eur. J. Inorg. Chem.*, 2007, **2007**, 4679–4686.
32 P. D. Hall, M. A. Stevens, J. Y. J. Wang, L. N. Pham, M. L. Coote and A. L. Colebatch, *Inorg. Chem.*, 2022, **61**, 19333–19343.
33 A. R. Delaney, L.-J. Yu, M. L. Coote and A. L. Colebatch, *Dalton Trans.*, 2021, **50**, 11909–11917.
34 A. R. Delaney, L.-J. Yu, V. Doan, M. L. Coote and A. L. Colebatch, *Chem. – Eur. J.*, 2023, **29**, e202203940.
35 A. J. H. Multem, A. R. Delaney, A. A. Kroeger, M. L. Coote and A. L. Colebatch, *Chem. – Asian J.*, 2024, **19**, e202301071.
36 H. Li, T. P. Gonçalves, D. Lupp and K.-W. Huang, *ACS Catal.*, 2019, **9**, 1619–1629.
37 M. Li, S. K. Gupta, S. Dechert, S. Demeshko and F. Meyer, *Angew. Chem., Int. Ed.*, 2021, **60**, 14480–14487.
38 A. Gers-Barlag, P. Goursot, M. Li, S. Dechert and F. Meyer, *Eur. J. Inorg. Chem.*, 2019, **2019**, 3329–3334.
39 C. P. Yap, Y. Y. Chong, T. S. Chwee and W. Y. Fan, *Dalton Trans.*, 2018, **47**, 8483–8488.
40 L. Yang, D. R. Powell and R. P. Houser, *Dalton Trans.*, 2007, 955–964.
41 Í. Ferrer, J. Rich, X. Fontrodona, M. Rodríguez and I. Romero, *Dalton Trans.*, 2013, **42**, 13461.
42 C. Sens, M. Rodríguez, I. Romero, A. Llobet, T. Parella, B. P. Sullivan and J. Benet-Buchholz, *Inorg. Chem.*, 2003, **42**, 2040–2048.
43 G. Gupta, G. P. A. Yap, B. Therrien and K. Mohan Rao, *Polyhedron*, 2009, **28**, 844–850.
44 A. Yoshinari, A. Tazawa, S. Kuwata and T. Ikariya, *Chem. – Asian J.*, 2012, **7**, 1417–1425.
45 T. Jozak, D. Zabel, A. Schubert, Y. Sun and W. R. Thiel, *Eur. J. Inorg. Chem.*, 2010, **2010**, 5135–5145.
46 D. Spasyuk and D. G. Gusev, *Organometallics*, 2012, **31**, 5239–5242.
47 J. Zhang, G. Leitus, Y. Ben-David and D. Milstein, *J. Am. Chem. Soc.*, 2005, **127**, 10840–10841.
48 B. Gnanaprakasam, J. Zhang and D. Milstein, *Angew. Chem., Int. Ed.*, 2010, **49**, 1468–1471.
49 C. Gunanathan and D. Milstein, *Acc. Chem. Res.*, 2011, **44**, 588–602.

50 A. C. Cabelof, V. Carta and K. G. Caulton, *Chem. Commun.*, 2021, **57**, 2780–2783.
51 O. Rivada-Wheelaghan, S. L. Aristizábal, J. López-Serrano, R. R. Fayzullin and J. R. Khusnutdinova, *Angew. Chem., Int. Ed.*, 2017, **56**, 16267–16271.
52 J. M. Blacquiere, *ACS Catal.*, 2021, **11**, 5416–5437.
53 D. Carmona, F. J. Lahoz, R. Atencio, A. J. Edwards, L. A. Oro, M. P. Lamata, M. Esteban and S. Trofimenko, *Inorg. Chem.*, 1996, **35**, 2549–2557.
54 I. Schlapp-Hackl, C. Hassenrück, K. Wurst, H. Kopacka, T. Müller, R. F. Winter and B. Bildstein, *Eur. J. Inorg. Chem.*, 2018, **2018**, 4434–4441.
55 C. Krüger, H. Sato, T. Matsumoto, T. Shiga, G. N. Newton, F. Renz and H. Oshio, *Dalton Trans.*, 2012, **41**, 11270.
56 J. Olguín and S. Brooker, *New J. Chem.*, 2011, **35**, 1242–1253.
57 S. Yadav and R. Gupta, *ACS Sustainable Chem. Eng.*, 2023, **11**, 8533–8543.
58 M. L. Rigsby, S. Mandal, W. Nam, L. C. Spencer, A. Llobet and S. S. Stahl, *Chem. Sci.*, 2012, **3**, 3058.
59 B. Cordero, V. Gómez, A. E. Platero-Prats, M. Revés, J. Echeverría, E. Cremades, F. Barragán and S. Alvarez, *Dalton Trans.*, 2008, 2832–2838.
60 A. Klein, B. Rausch, A. Kaiser, N. Vogt and A. Krest, *J. Organomet. Chem.*, 2014, **774**, 86–93.
61 C. Yoo and Y. Lee, *Angew. Chem., Int. Ed.*, 2017, **56**, 9502–9506.
62 D. Sahoo, C. Yoo and Y. Lee, *J. Am. Chem. Soc.*, 2018, **140**, 2179–2185.
63 S. Lapointe, E. Khaskin, R. R. Fayzullin and J. R. Khusnutdinova, *Organometallics*, 2019, **38**, 1581–1594.
64 S. Feng, J. Chen, R. Wang, H. Li, J. Xie, Z. Guo, T.-C. Lau and Y. Liu, *J. Am. Chem. Soc.*, 2024, **146**, 21490–21495.
65 T. Toda, A. Yoshinari, T. Ikariya and S. Kuwata, *Chem. – Eur. J.*, 2016, **22**, 16675–16683.
66 N. Ahmad, J. J. Levison, S. D. Robinson, M. F. Uttley, E. R. Wonchoba and G. W. Parshall, *Inorg. Synth.*, 1974, **15**, 45–64.
67 P. S. Hallman, T. A. Stephenson and G. Wilkinson, *Inorg. Synth.*, 1970, **12**, 237–240.
68 *CrysAlisPRO*, Oxford Diffraction/Agilent Technologies UK Ltd., Yarnton, England, 2020.
69 G. M. Sheldrick, *Acta Crystallogr., Sect. A: Found. Adv.*, 2015, **71**, 3–8.
70 G. M. Sheldrick, *Acta Crystallogr., Sect. C: Struct. Chem.*, 2015, **71**, 3–8.
71 O. V. Dolomanov, L. J. Bourhis, R. J. Gildea, J. A. K. Howard and H. Puschmann, *J. Appl. Crystallogr.*, 2009, **42**, 339–341.